JOURNAL OF THE ROYAL SOCIETY Interface

rsif.royalsocietypublishing.org

Research

Cite this article: Lehnert MS, Monaenkova D, Andrukh T, Beard CE, Adler PH, Kornev KG. 2013 Hydrophobic–hydrophilic dichotomy of the butterfly proboscis. J R Soc Interface 10: 20130336.
http://dx.doi.org/10.1098/rsif.2013.0336

Received: 12 April 2013
Accepted: 20 May 2013

Subject Areas:
biomaterials, biophysics, biomechanics

Keywords:
Lepidoptera, proboscis, wettability, cleaning, capillary rise, Cassie–Baxter theory

Author for correspondence:
Konstantin G. Kornev
e-mail: kkornev@clemson.edu

†These authors contributed equally to this study.

Electronic supplementary material is available at http://dx.doi.org/10.1098/rsif.2013.0336 or via http://rsif.royalsocietypublishing.org.

Royal Society Publishing
Informing the science of the future

Hydrophobic–hydrophilic dichotomy of the butterfly proboscis

Matthew S. Lehnert[1,3,†], Daria Monaenkova[2,4,†], Taras Andrukh[2], Charles E. Beard[1], Peter H. Adler[1] and Konstantin G. Kornev[2]

[1]School of Agricultural, Forest and Environmental Sciences, and [2]Department of Materials Science & Engineering, Clemson University, Clemson, SC 29634, USA
[3]Department of Biological Sciences, Kent State University, North Canton, OH 44720, USA
[4]School of Physics, Georgia Institute of Technology, Atlanta, GA 30332, USA

Mouthparts of fluid-feeding insects have unique material properties with no human-engineered analogue: the feeding devices acquire sticky and viscous liquids while remaining clean. We discovered that the external surface of the butterfly proboscis has a sharp boundary separating a hydrophilic drinking region and a hydrophobic non-drinking region. The structural arrangement of the proboscis provides the basis for the wetting dichotomy. Theoretical and experimental analyses show that fluid uptake is associated with enlargement of hydrophilic cuticular structures, the legulae, which link the two halves of the proboscis together. We also show that an elliptical proboscis produces a higher external meniscus than does a cylindrical proboscis of the same circumference. Fluid uptake is additionally facilitated in sap-feeding butterflies that have a proboscis with enlarged chemosensory structures forming a brush near the tip. This structural modification of the proboscis enables sap feeders to exploit films of liquid more efficiently. Structural changes along the proboscis, including increased legular width and presence of a brush-like tip, occur in a wide range of species, suggesting that a wetting dichotomy is widespread in the Lepidoptera.

1. Introduction

The success of insects—about two-thirds of all known species on Earth [1]—reflects the evolutionary integration of chemistries, natural materials, and physical properties into devices, such as mouthparts, that address multiple, often conflicting, demands. Feeding from nutrient-rich resources as diverse as floral nectar, dung and sap presents butterflies and moths (Lepidoptera), the premiere fluid feeders [2], with the dual challenge of acquiring fluids while maintaining a clean proboscis free of sticky fluids and adherent debris [3] that could impede fluid uptake and sensory input. Hydrophobic chitin in the cuticle of the mouthparts [4], coupled with surface lipids, waxes [5,6] and roughness, would significantly decrease the surface energy of the proboscis [7] and facilitate cleaning [8–10], but would hinder its wettability [11–13].

Lepidopteran feeding habits and the material properties of the proboscis are, therefore, contradictory: how does a proboscis with hydrophobic properties acquire aqueous fluids? We provide the first experimental demonstration of a wetting–non-wetting dichotomy of insect mouthparts, which is achieved in butterflies by structural differentiation of the proboscis. The proboscis features a subdivision of hydrophobic and hydrophilic regions not previously reported in other organisms [14,15].

2. Proboscis structure

The lepidopteran proboscis is composed of two elongated strands, the galeae, with C-shaped cross sections that form a food canal [12,16,17]. The two strands are joined by cuticular projections, the legulae, which arise from the top (dorsal) and bottom (ventral) medial edges of each galea; the dorsal legulae overlap and

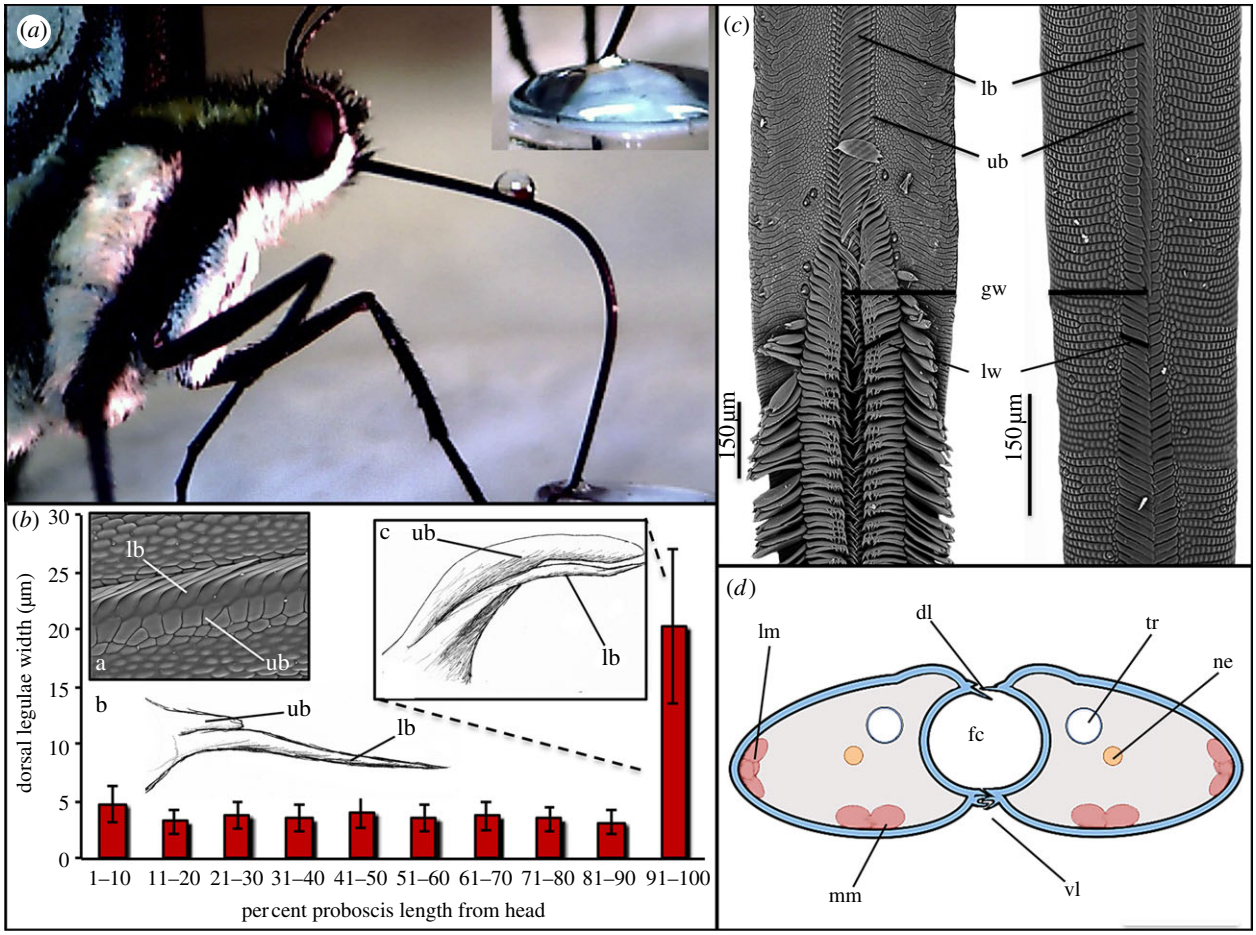

Figure 1. Structural features and wettability of the lepidopteran proboscis. (*a*) Water droplet placed on the proximal region of the proboscis of *Papilio glaucus* results in a clam-shell formation, indicating hydrophobicity, whereas fluid on the submersed distal region of the proboscis has a hydrophilic contact angle (inset). (*b*) The dorsal legulae remain approximately the same width along 90 per cent of the proboscis of *Danaus plexippus*. Each dorsal legula consists of an upper (ub) and lower branch (lb; insets a,b); the upper branches enlarge in the distal region of the proboscis (inset c). (*c*) We measured the widths of the upper branch of the legula (lw) and the galea (gw) to demonstrate structural arrangements of brush-tipped and smooth-tipped proboscises (*Limenitis arthemis astyanax* proboscis on the left, with slight artefactual opening between dorsal legulae of opposing galeae; *Danaus plexippus* on the right). (*d*) Schematic of a cross section of the proboscis showing two C-shaped galeae with lateral and median intrinsic muscles (lm and mm, respectively), nerves (ne) and tracheae (tr). The galeae are held together by overlapping dorsal legulae (dl) and interlinking ventral legulae (vl), forming a food canal (fc). (Online version in colour.)

the ventral legulae interlink, forming a functional proboscis. The dorsal legulae of the terminal 5–20% of the proboscis are enlarged and widely spaced [16], and are applied to pools or films of liquid when feeding [12] (figure 1*a*). Liquid enters the proboscis through the spaces between the dorsal legulae [12]. Each dorsal legula consists of an upper and lower branch (figure 1*b*,*c*). The lower branches overlap and are wider than the upper branches, except in the terminal 5–20% of the proboscis, where the upper branches and interlegular spaces enlarge (figure 1*b*,*c*). The cross section of the proboscis can be approximated by an ellipse; for instance, the proboscis of the monarch butterfly has the longer axis of the ellipse, *a*, about twice the length of the shortest axis, *b* (figures 1*d* and 4*b*).

Proboscis structure is related to feeding habits. Sap-feeding butterflies, for instance, have enlarged chemosensory structures (chemosensilla) near the tip of their proboscises. These chemosensilla give the proboscis a brush-like appearance that putatively aids in feeding on liquid films [17,18]; the brush is lacking or reduced in typical nectar feeders [19]. The structural modifications of the proboscis add to a list of challenges in studies of wettability [20–22]. The few experimental studies of insects supported by theoretical analysis of wetting phenomena [13,15,23–25] do not address insect mouthparts. We use a capillary-rise technique with the lepidopteran proboscis to show the natural solution for producing a fibre surface with dichotomous hydrophobic–hydrophilic features.

3. Scanning the wettability of the external surface of the proboscis

When a vertical proboscis pierces a water–air interface, a meniscus forms around it. The meniscus meets the proboscis surface at contact angle θ, which depends on the structure and materials chemistry of the proboscis [7]. The meniscus approaches a horizontal water–air interface as the distance from the proboscis increases; the shape of the meniscus and its height are important physico-chemical parameters allowing the proboscis wettability to be evaluated. An analysis based on the capillary rise of an external meniscus [26] makes it possible to examine contact angles greater than approximately 60° where the traditional drop-on-fibre technique is inadequate [27]) (figure 2*a*). In our experiments, the wettability of the proboscis surface of four to seven butterflies for each of five species was scanned by raising the water level in a dish and video recording the shape of the meniscus (figure 2*a*).

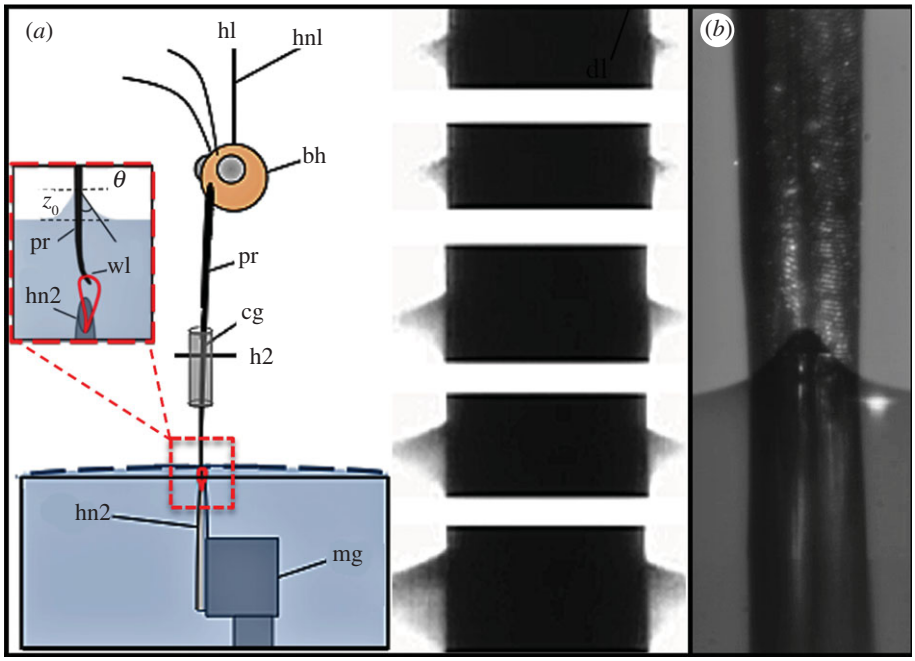

Figure 2. Interactions between proboscises and water. (*a*) Schematic of the capillary-rise technique showing the butterfly head (bh), proboscis (pr) threaded through a capillary tube (cg), hypodermic needle (hn1), manually-controlled holder (h1), tungsten wire loop (wl) against which the proboscis was held, second hypodermic needle (hn2), magnets (mg), height (z_0) of the contact meniscus and contact angle (θ). Individual video frames (vertical series on right) were used to assess the height (z_0) of the contact meniscus and the contact angle (θ) at the proximal area of the drinking region; the bottom images represent distal regions of the proboscis and the top image is near the hydrophilic–hydrophobic junction. The frame depicting the demarcation is not shown because the visible upward meniscus disappeared, indicating the 90° angle. (*b*) Liquid finger on the dorsal legulae of the proboscis. (Online version in colour.)

We previously showed by X-ray phase-contrast imaging that the food canal is hydrophilic: stable liquid menisci form contact angles of approximately 45° [12]. In our capillary-rise experiments used here, when the tip of the proboscis contacted the water–air interface, water entered the wettable food canal at the rate of 6–20 mm s^{-1} (see the electronic supplementary material, movie). After the food canal was filled with water, the external meniscus acquired an equilibrium configuration with an acute contact angle around the external surface of the proboscis.

As the height of the water in the dish increased and the contact line moved up, the initial acute contact angle of the meniscus of all 25 tested butterflies shifted to 90°, indicated by a flat water–air interface (figure 2*a*). Raising the water level further, we observed that the contact line had moved up but the meniscus formed a circular dimple. Hence, the overall surface wettability of the proboscis shifted from hydrophilic to hydrophobic and the meniscus formed a contact angle greater than 90°. The sharp demarcation between the wetting and non-wetting regions allowed us to quantitatively classify the hydrophilic section as a drinking region (5–17% of the proboscis length in our butterflies, depending on species) and the hydrophobic section as a non-drinking region. By inverting butterfly heads ($n = 3$) in water and observing menisci for water and upside-down proboscises, we confirmed that there was no contact angle hysteresis; the boundary of the drinking region was detected at the same level as in the initial submersion experiments.

The dorsal legulae facilitated droplet entry into the food canal, suggesting that they are hydrophilic. To further evaluate this hypothesis, we used Nile red for its ability to fluoresce a range of hydrophobic and lipid-rich materials. The dorsal legulae, food canal and brush-like chemosensilla did not bind with Nile red, suggesting that they are hydrophilic, in contrast to the overall hydrophobicity of the adjacent galeal surface (figure 3*a*). The staining pattern implies that enlarged hydrophilic legulae interspersed with larger spaces promote fluid uptake in the drinking region, and the brush of sap-feeding butterflies further enhances hydrophilicity.

In our study, all dynamic effects of meniscus movement and interactions of external and internal menisci were set aside, and we focused on the analysis of stationary external menisci coexisting with the liquid-filled food canal. The measurements were taken after complete equilibration of the external meniscus, suggesting that the liquid column filling the food canal had already reached the head, eliminating any internal meniscus. By studying external menisci in the drinking region, we observed that the liquid-filled food canal, in combination with the larger interlegular spaces, resulted in the formation of a heightened meniscus on the dorsal legulae, which did not encircle the whole proboscis (figure 2*b*). If the entire external surface of the proboscis in the drinking region were hydrophilic, no finger-like meniscus would appear; the external meniscus would envelop the whole proboscis [28]. In our experiments, however, the meniscus contact line moved faster along the dorsal legulae than over the remainder of the proboscis, leaving the galeal exterior dry, which suggests that the exterior of the proboscis is predominantly hydrophobic. When the water surface approached the proximal boundary of the drinking region, the meniscus expanded around the sides and embraced the proboscis surface completely.

The existing model of capillary rise cannot be applied directly to the proboscis meniscus, because it was developed only for a circular fibre [26,28]. A new model is required to quantitatively analyse and explain the change in contact angle near the well-defined wetting–non-wetting transition. We present a new model for analysing contact angles on elliptical fibres.

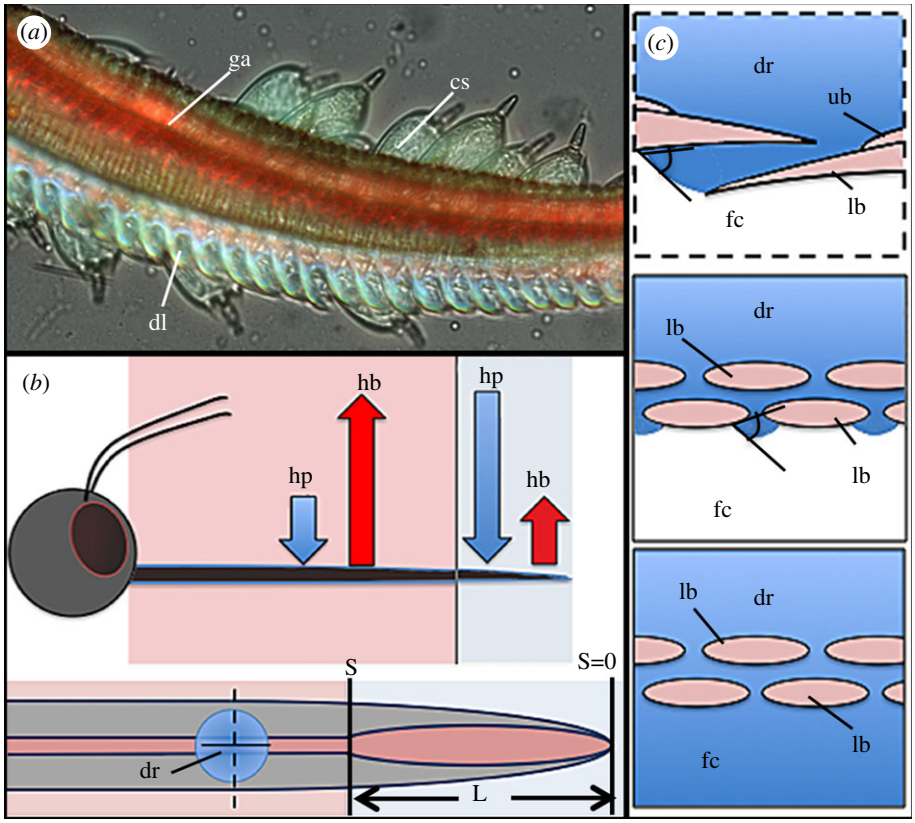

Figure 3. Overall wettability of the proboscis. (*a*) Proboscis of the red-spotted purple stained with Nile red revealed hydrophilic chemosensilla (cs) and dorsal legulae (dl; blue) and overall hydrophobic galeae (ga; red). (*b*) Summary hydrophobic (hb) and hydrophilic (hp) forces in the non-drinking region (pink) and drinking region (blue). Arrows representing forces are not to scale. The bottom schematic shows a droplet (dr) on the non-drinking region with sections (dashed line is cross section, solid is sagittal) that are enlarged in (*c*). Position S is the proximal portion of the drinking region where the height of the contact meniscus and contact angle were assessed, which was measured from the proboscis tip ($S = 0$) to determine the total length of the drinking region (L). (*c*) A cross section of the proboscis (top image with dashed frame) and sagittal section (middle and bottom images) demonstrate a metastable state for a droplet on the non-drinking region when the food canal is empty: the legulae are hydrophilic; hence, the meniscus forms an acute angle and supports the formation of a film in the food canal. The droplets eventually enter the food canal (bottom image).

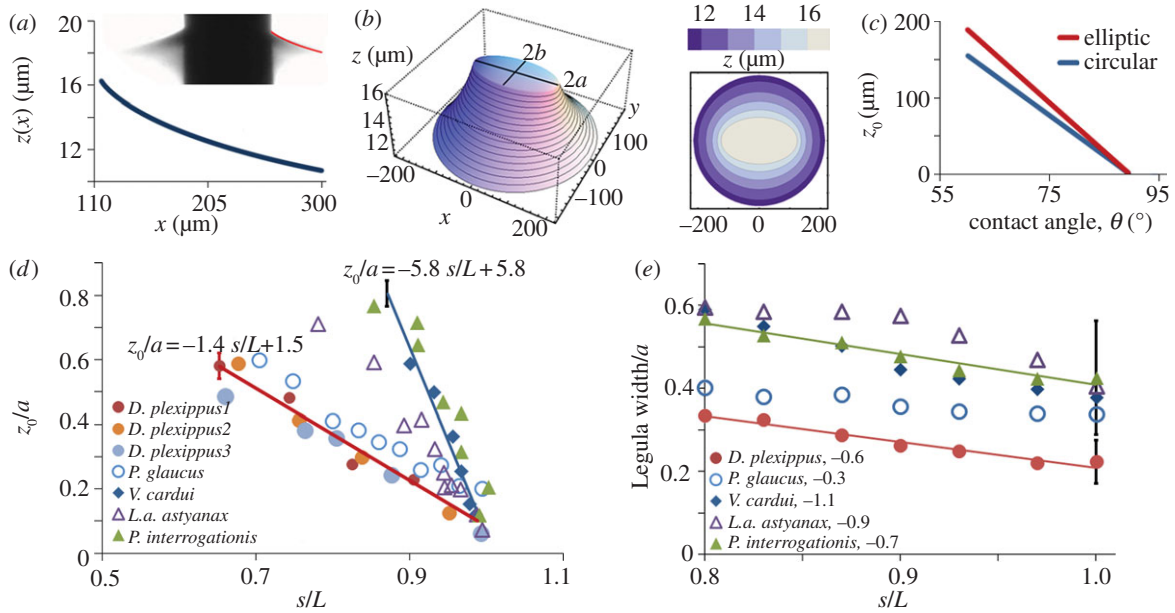

Figure 4. Wetting properties of proboscises with elliptical or circular cross sections. (*a*) Profile of the liquid meniscus near the drinking region in the $z-y$ central cross section (a = 116 μm, b = 50 μm, 87° contact angle). The inset shows the meniscus overlaid with the experimental result. (*b*) Three-dimensional profile of the liquid meniscus on an elliptical proboscis (*Danaus plexippus*) (left) and corresponding contour map of liquid elevation heights (right). (*c*) Comparison of the maximum elevation height, z_0, of the meniscus on an elliptical proboscis (a = 135 μm, b = 56 μm) and circular proboscis of the same perimeter ($R = 100$ μm) at different contact angles. (*d*) Experimental results of elevation heights of menisci (z_0/a) for different species versus meniscus position with respect to the tip of the proboscis (s/L) ($n = 3$ for each point s). The distance from the tip is normalized by the length of the drinking region, L. The graph shows clustering of experimental data for butterflies with smooth and brush-tipped proboscises. The linear fit (solid lines) gives the variation of the rates of the surface wettability along the proboscis. (*e*) Normalized width of the dorsal legulae of the proboscis versus the distance from the proboscis tip to the measured legulae acquired from SEM images and the slopes of linear trend lines ($n = 3$ per species).

4. Meniscus on an elliptical fibre: problem formulation and results

The region of the proboscis where the wetting demarcation occurs was magnified to reveal the profile of the meniscus for quantification. In the Cartesian system of coordinates (z,x,y), the meniscus profile $z = S(x,y)$ describes the liquid elevation above the reference plane (x,y), which coincides with the horizontal water level away from the area of interaction between the proboscis and water. The centre of coordinates is chosen at the ellipse axis. The Laplace law of capillarity is employed to describe the meniscus shape [7]:

$$\sigma\nabla\cdot\left(\frac{\nabla S}{(1+(\nabla S)^2)^{1/2}}\right)-\rho g S=0, \tag{4.1}$$

where σ is the surface tension of the liquid, ρ is the liquid density, g is the acceleration due to gravity and $\nabla = (\partial/\partial x, \partial/\partial y)$ is the two-dimensional gradient operator. The proboscis is modelled as an elliptical cylinder with the cross-sectional profile described by the following equation: $(x/a)^2 + (y/b)^2 = 1$, where a and b, $a > b$, are the major and minor semi-axes of the ellipse. In our experiments, the meniscus height S was nearly constant. At infinity, the meniscus approaches the flat water–air interface. We, therefore, formulated the following boundary conditions:

$$S = S_0 \quad \text{at } \left(\frac{x}{a}\right)^2+\left(\frac{y}{b}\right)^2=1; \quad S\to 0 \quad \text{as } x^2+y^2\to\infty. \tag{4.2}$$

Two length scales are associated with this problem. One is the capillary length, $l_c = (\sigma/\rho g)^{1/2}$, and the other is the major ellipse semi-axis, a. Introducing the dimensionless variables as follows, $(x, y)\to(x/a, y/a) = (X, Y)$, and function $Z = S/a$, we rewrite equations (4.1) and (4.2) in the dimensionless form as

$$\nabla\cdot\left(\frac{\nabla Z}{(1+(\nabla Z)^2)^{1/2}}\right)-\varepsilon Z=0 \quad \text{and} \quad \varepsilon=\frac{\rho g a^2}{\sigma}=\frac{a^2}{l_c^2}, \tag{4.3}$$

$$Z = Z_0 \quad \text{at } (X)^2+(Y\frac{a}{b})^2=1; \quad Z\to 0 \quad \text{as } X^2+Y^2\to\infty. \tag{4.4}$$

To find a relation between the meniscus height and average contact angle, we use the force balance equation, which follows from equation (4.3). Integrating equation (4.3) over the exterior of the proboscis, we obtain

$$\begin{aligned}\int\nabla\cdot\left(\frac{\nabla Z}{(1+(\nabla Z)^2)^{1/2}}\right)\mathrm{d}x\,\mathrm{d}y-\int\varepsilon Z\,\mathrm{d}x\,\mathrm{d}y&\\ =-\oint\frac{\partial Z}{\partial n}\left(1+\left(\frac{\partial Z}{\partial n}\right)^2\right)^{-1/2}\mathrm{d}l-\int\varepsilon Z\,\mathrm{d}x\,\mathrm{d}y&\\ =l\cos\theta-\int\varepsilon Z\,\mathrm{d}x\,\mathrm{d}y=0,&\end{aligned} \tag{4.5}$$

where the contour integral is taken over the proboscis surface, l is the fibre perimeter and $\cos\theta$ is the cosine of the contact angle averaged over the fibre perimeter.

Equation (4.3) can be simplified, taking into account that when the meniscus disappears in the transition region, the contact angle is close to $\pi/2$. The maximum slope is reached at the fibre surface; therefore, we assume that the slopes of the free surface outside the fibre are even smaller, $|\nabla Z| \ll 1$. This observation allows equation (4.3) to be simplified as

$$\Delta Z-\varepsilon Z=0, \tag{4.6}$$

where $\Delta = (\partial^2/\partial X^2 + \partial^2/\partial Y^2)$ is the two-dimensional Laplace operator. Proboscises of Lepidoptera are thin, i.e. the inequality $\varepsilon = \rho g a^2/\sigma \ll 1$ holds true, implying that the shape of the meniscus is controlled primarily by capillary forces and gravity plays a secondary role in shaping the meniscus. Therefore, an approximate solution to the boundary value problem (4.4)–(4.6) can be constructed using the technique of matched asymptotic expansions as proposed by Lo [28].

In §6, we obtained an asymptotic solution for model (4.4)–(4.6). An asymptotic analysis of the meniscus shape results in the formula for the meniscus height at the point s measured from the submersed tip

$$z_0\left(\frac{s}{L}\right)=\left(\frac{al\delta}{2\pi}\right)\left\{\ln\left(\frac{(1+b/a)\sqrt{\varepsilon}e^{\gamma}}{4}\right)\right\}, \tag{4.7}$$

where $\delta = \theta(s/L) - \pi/2$, $|\delta| \ll 1$, $\theta(s/L)$ is the average contact angle at the given point s along the proboscis and $\gamma = 0.577215$ is the Euler constant. An elliptical proboscis, thus, provides a higher meniscus, compared with a cylindrical proboscis of the same circumference (figure 4*c*). At the asymptotic limit, as the b/a ratio tends to 1, the meniscus height approaches that on a cylinder, $z_0 \approx a\delta\ln(\sqrt{\varepsilon}e^{\gamma}/2)$, which coincides with the Lo solution [28] when $\theta \approx \pi/2$. The observation that greater ellipticity results in a higher meniscus has not been discussed in the engineering literature, yet is important for the design of probes and other microfluidic devices [29]. The meniscus profile is also obtained analytically and is given in §6. Using the derived formulas, we can extract the average contact angle from the images and analyse its dependence on the proboscis structure near the transition region.

5. Effect of proboscis structure on contact angle

On smooth surfaces, the equilibrium contact angle θ between a wetted solid surface and a droplet is defined by the interfacial tensions of co-existing phases through Young's equation, but this equation is not valid for the rough surfaces of lepidopteran proboscises. Young's equation, therefore, requires corrections [30–37]. The Cassie–Baxter equation [30,35] accounts for surface heterogeneity and can be applied to butterfly proboscises.

When a droplet meets a rough surface interspersed with air pockets, the contact angle of the droplet exceeds 90° because the non-wettable air prevents the droplet from spreading. When the food canal is free of fluid, dorsal legulae separated by air spaces similarly can be modelled with the Cassie–Baxter equation. A droplet captured by the proboscis surface will be prevented from entering the food canal by a liquid–air interface that bridges the legulae via local menisci, resulting in an effectively hydrophobic interaction (figure 3*b*,*c*). This model holds even if the smooth dorsal legulae are hydrophilic, as a droplet can bead on a hydrophilic fibre with contact angle less than 90° [38,39]; therefore, a cylindrical proboscis with hydrophilic legulae can be effectively hydrophobic (figure 3*b*). The unfilled food canal, however, is open to air that enters and exits at multiple sites. A droplet on the dorsal legulae causes a capillary-pressure differential that results in the droplet

Table 1. Measurements of model parameters for tested butterflies ($n = 3$/species).

species	a (μm)	b (μm)	z_0'/a	D/a	$L\,\mathrm{d}f/\mathrm{d}s$
Danaus plexippus	135	56	−1.43	1.11	−1.29
Papilio glaucus	182	65	−1.37	1.00	−1.37
Vanessa cardui	105	36	−5.78	1.16	−4.96
Limenitis arthemis astyanax	252	32	−3.08	0.87	−3.55
Polygonia interrogationis	149	48	−4.54	1.05	−4.32

entering the food canal [12]. The air between overlapping dorsal legulae and the smaller interlegular spaces (96 ± 27 nm) of the non-drinking region would kinetically delay a droplet entering the food canal relative to the larger spaces (2 ± 1 μm) between the dorsal legulae of the drinking region (figure 3*b*,*c*) [12].

5.1. Legular structure and interlegular spacing at the wetting transition

An increase in size of the dorsal legulae mirrored the change in proboscis wettability. In the non-drinking region, the lower legular branches overlap and are wider than the upper branches. The upper branches, however, enlarge in the drinking region, as do the interlegular spaces, coinciding with the change in wettability (figure 1*b*,*c*; table 1). The structural shift of dorsal legulae from tightly spaced and overlapping in the non-drinking region to non-overlapping and more widely spaced in the drinking region changes the surface roughness, influencing liquid entry into the food canal.

The galeal surfaces are made of bumps and valleys (figure 1*b*, inset). When water moves over the galeal surfaces, it first penetrates the valleys, and two adjacent water-filled valleys are bridged by the water arc covering the bump (unpublished video). Therefore, we apply the Cassie model [35–37,40], assuming that the visible macroscopic contact line moves not over a complex topography, but over a functionally smooth surface. This smooth surface is chemically heterogeneous: it is composed of water-filled valleys, with $\theta_{\mathrm{philic}} = 0$, and surfaces of polymer bumps [40]. We also assume that near the transition region, the polymer bumps provide $\theta_{\mathrm{phobic}} \sim \pi/2$. Introducing a fractional area f of the proboscis surface covered with water, we can write the Cassie equation as $\cos\theta = f \cdot \cos\theta_{\mathrm{philic}} + (1-f)\cos\theta_{\mathrm{phobic}} \sim f$. Just above the demarcation where $|\delta - \pi/2| \ll 1$, this equation can be represented as $\cos(\theta \pm \pi/2) = -\sin\delta \approx -\delta \approx f$; therefore, we obtain from equation (4.7) the rate of decrease of the water-filled valleys when we move the distance ds proximally from the drinking region where a and b do not change significantly:

$$\frac{\mathrm{d}f}{\mathrm{d}s} = \frac{\mathrm{d}z_0/\mathrm{d}s}{-(al/2\pi)\,\ln((1+b/a)\cdot\sqrt{\varepsilon}e^{\gamma}/4)}. \qquad (5.1)$$

As shown in our experiments, meniscus height z_0 near the boundary of the drinking region changes linearly with the distance from the proboscis tip. From equation (5.1), it follows that the fractional area of hydrophilic valleys also should be a linear function of s. Using our capillary-rise data, we estimated the derivative $\mathrm{d}z_0/\mathrm{d}s$ and, based on scanning electron microscope images, we calculated the factor $D = -(al/2\pi)\ln((1+b/a)\cdot\sqrt{\varepsilon}e^{\gamma}/4)$. Table 1 summarizes the data for all butterflies where the derivative $z_0' = \mathrm{d}(z_0/a)/\mathrm{d}(s/L)$ was taken from the slopes in figure 4.

The experimental data of z_0/a versus s/L are shown in figure 4*d*. The data for nectar-feeding monarchs (*Danaus plexippus*) and eastern tiger swallowtails (*Papilio glaucus*) cluster separately from those for sap-feeding butterflies with brush-tipped proboscises (table 1). The $L\,\mathrm{d}f/\mathrm{d}s$ derivatives for nectar feeders are similar to each other, suggesting the same mechanism of wettability change. The sap feeders have a faster rate of increase for the hydrophilic area as distance to the tip decreases. The association of wettability change with a change in surface roughness is reflected by the relation of legular width versus length in the drinking region, which shows the same slope for all species (figure 4*e*). The interlegular spacing versus length of the drinking region would be expected to show a similar trend; therefore, in nectar feeders, the hydrophilicity can be associated primarily with legular structure, whereas sap feeders rely not only on the change in legular pattern, but also on the enlarged chemosensilla that form the brush-like tip.

The higher meniscus of an elliptical proboscis provides a possible functional role for the differences in proboscis shape among species. Our sap-feeding butterflies have more elliptical proboscises than do the nectar feeders. An elliptical proboscis with a portion of the drinking region enveloped with liquid will bring the contact line of the meniscus higher on the drinking region than will a cylindrical proboscis, resulting in more interlegular spaces covered with liquid, which would support liquid-bridge formation in the food canal [12]. Sap feeders, thus, are better adapted to exploit films of liquid. In sap feeders, the change from the non-drinking to the drinking region is accompanied by the abrupt appearance of brush-like chemosensilla, further increasing the ellipticity of the proboscis.

5.2. Conclusions. Reconciling drinking and cleaning

Differential wettability of the cuticle is widespread among insects, although previously investigated experimentally only for legs and wings [41–43]. Fluid-feeding insects faced with the paradox of drinking liquids while repelling adherent films and debris have solved the challenge by exploiting an overall wettability dichotomy. We suggest that the factors influencing overall hydrophobicity of the non-drinking region—overlapping dorsal legulae, reduced interlegular spaces, lack of enlarged chemosensilla, small upper branches of dorsal legulae—promote cleaning and inhibit the adherence of pollen, sap and other substances that could affect feeding ability and reduce the functionality of sensory structures.

Structural features such as the transition in legular size and spacing is found in a wide range of Lepidoptera [44–46], suggesting that the wettability dichotomy is widespread in this order of insects. Micro-scale patterns of

wettability associated with additional structural features, such as the micro-bumps and valleys on the galeae, might further fine tune the channelling of fluids while still permitting self-cleaning. Cuticular surface sculpturing is a characteristic property of the mouthparts of fluid-feeding insects [16], including members of ancient lineages [44].

The principles of cuticular wettability demonstrated for butterflies should have adaptive value in directing and channelling fluids for uptake while maintaining a clean surface in all fluid-feeding insects—more than half of Earth's known species [1,2]. These principles offer a new perspective to explain fluid feeding, which complement existing macroscale studies that indicate the presence of a drinking region in a broad range of insects [3,18,47–49]. We suggest that the physical principles associated with fluid uptake and cleaning—variation in surface roughness, ellipticity, distribution of wetting chemistry, and size and arrangement of air spaces—influence liquid acquisition in all fluid-feeding insects. Variations in these characters could have facilitated diversification of feeding habits and influenced the adaptive radiation of fluid-feeding insects. The wetting properties of the butterfly proboscis can provide similar strategies for the development of micro- and nanofluidic probes [29].

6. Material and methods

6.1. Test species

Monarchs (*Danaus plexippus*) (Shady Oak Butterfly Farm, Brooker, FL) were obtained as adults or pupae, and painted ladies (*Vanessa cardui*) (Carolina Biological Supply Co., Burlington, NC) were reared on an artificial diet. Eastern tiger swallowtails (*Papilio glaucus*), red-spotted purples (*Limenitis arthemis astyanax*) and question marks (*Polygonia interrogationis*) collected August–September 2011 around Clemson, SC (34°39′ N 82°50 W) were reared on leaves of tulip trees (*Liriodendron tulipifera*), black cherry (*Prunus serotina*) and winged elm (*Ulmus alata*), respectively, in plastic dishes (Rubbermaid TakeAlongs, Atlanta, GA). All species were reared at $24 \pm 2^{\circ}$C and relative humidity of 60–80%, with a 15 : 9 photo:scotophase under 100 W incandescent lights. Each specimen was placed in a glassine envelope 24 h after emergence and held at -74°C for at least 1 h before wettability experiments. To prevent chemical contamination of the proboscis, unfed, laboratory-reared specimens were handled with latex gloves. Voucher specimens were deposited in the Clemson University Arthropod Collection.

6.2. Microscopy and staining

Butterfly heads (four to seven per species) that we used in wettability experiments subsequently were secured on Styrofoam and their proboscises straightened with insect pins. The heads with extended proboscises were dehydrated in an ethanol series (80, 95, 100%, approximately 24 h each), soaked in hexamethyldisilazane, air-dried, attached to mounts with carbon-graphite adhesive tape and sputter coated with platinum for 1–2 min. A Hitachi TM-3000 Scanning Electron Microscope in composite mode was used to take a series of photographs along the dorsum of the entire proboscis at 80× magnification, 15 kV and full vacuum. An additional series of images was obtained for the distal one-quarter of the proboscis at either 200× or 300× and at 500×. Composite images were created from the serial images in Adobe Photoshop Elements, and opened in ImageJ software (http://rsbweb.nih.gov/ij/download.html) to acquire measurements. Butterfly proboscises ($n = 7$) were fluorescently stained in diluted Nile red [50] (Acros Organics 415711000; final concentration 5 μm ml^{-1} in aqueous glycerol) and imaged with a Nikon Eclipse Ti confocal microscope. A spectral analysis was used to distinguish Nile red from autofluorescence and to confirm staining.

6.3. Defining wettability regions

Video recordings were used to isolate the frame in which the contact angle θ between the distilled water and the proboscis was approximately 90° (transition from an acute to an obtuse angle). To measure the distance from the tip of the proboscis to the transition, we overlapped a frame showing the initial position of the proboscis with the corresponding frame for the transition zone in ImageJ software. To account for any error in estimating the transition, three researchers independently repeated the process of isolating the transition frame. Each researcher made two measurements per image in ImageJ software on each of two butterflies per species, using different points of the tungsten wire loop for calibration. A random effects model with the terms specimen, frame (specimen), evaluator (specimen × frame) and multiple (repeat) were used to determine a standard deviation, which then defined a region where the contact angle changed from acute to obtuse.

A measurement from the tip of the proboscis to the transition point was transferred to the corresponding SEM image (200× or 300×) of that same individual; SEM and wettability images were at the same scale. The calculated standard deviation represented the boundaries of the error in measuring the distance from the tip to the transition. A region equal in length to two standard deviations was added to the transition region proximally (hydrophobic) and distally (hydrophilic) (figure 5). Two structural measurements were made in each region on a single galea: (i) width of the upper branch of the dorsal legulae and (ii) width of the galea (table 2). Eight randomly selected dorsal legulae were measured in all three zones for each specimen, except the painted ladies (four dorsal legulae).

6.4. Asymptotic solution of model (4.4)–(4.6)

Following Lo [28], we seek an asymptotic solution by matching two asymptotic series, inner and outer, to find the necessary constants. The inner expansion describes the meniscus profile near the fibre while the outer expansion describes the meniscus profile far away from the fibre where it meets the horizontal air–water interface. Each solution contains one unknown constant which is obtained by matching two solutions in an intermediate zone where the solutions overlap.

Inner expansion. Closer to the fibre surface, equation (4.6) is rewritten as

$$\Delta Z = 0. \tag{6.1}$$

This equation can be solved by introducing the elliptical coordinates as

$$X = H\cosh\,\mu\cos\,v, \quad Y = H\sinh\,\mu\sin\,v,$$

where $2H$ is the normalized interfocal distance of the ellipse

$$\left.\begin{aligned} H = \frac{h}{a} = (1 - \frac{b^2}{a^2})^{1/2}, \quad 1 = H\cosh\,\mu_0, \\ b/a = H\sinh\,\mu_0, \quad \mu_0 = \left(\frac{1}{2}\right)\ln\left[\frac{1 + a/b}{a/b - 1}\right] \end{aligned}\right\}. \tag{6.2}$$

Equation (6.1) is rewritten as

$$\frac{(\partial^2 Z/\partial\mu^2) + (\partial^2 Z/\partial v^2)}{H^2(\sinh^2\,\mu + \sin^2\,v)} = 0 \quad \text{or} \quad \frac{\partial^2 Z}{\partial\mu^2} + \frac{\partial^2 Z}{\partial v^2} = 0. \tag{6.3}$$

Due to symmetry, one can solve equation (6.3) in the first quadrant, $0 < v < \pi/2$ using the following boundary conditions, $\partial Z/\partial v = 0$, $v = 0$ and $v = \pi/2$. The solution is

$$Z = K(\mu - \mu_0) + Z_0, \tag{6.4}$$

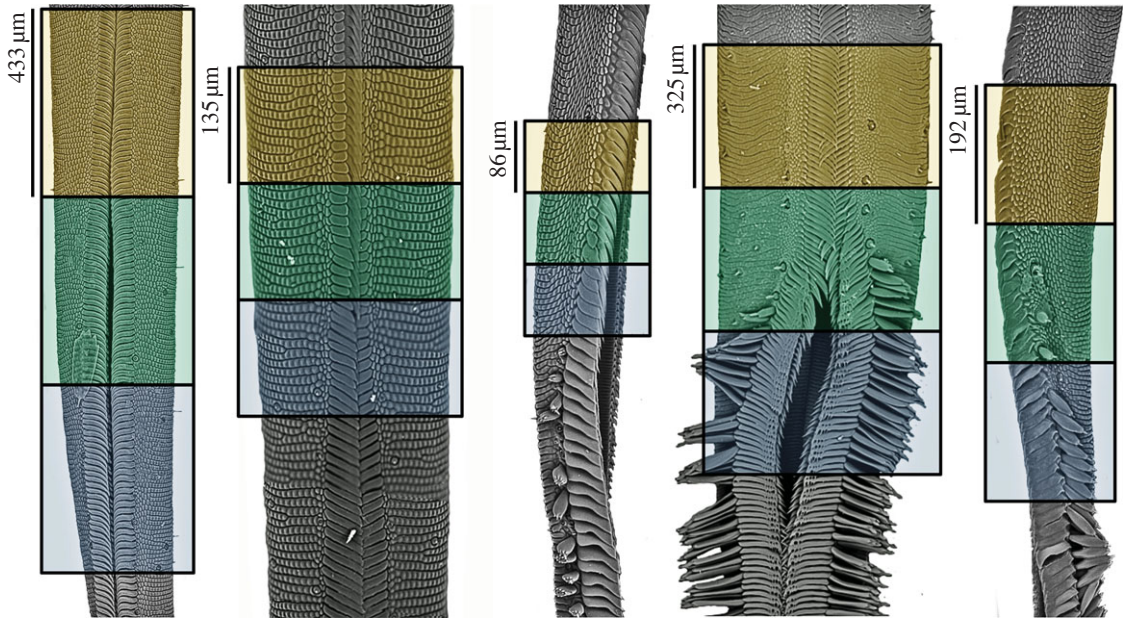

Figure 5. Scanning electron micrographs of butterfly proboscises and associated wettability regions. The upper (orange), middle (green) and lower (blue) blocks represent hydrophobic, transition and hydrophilic regions, respectively. A single galea is shown for *V. cardui* and *P. interrogationis*; both galeae are shown for other species. Gap between galeae of *L. arthemis astyanax* is an artefact.

Table 2. Measurements (mean ± s.e.) (µm) in non-drinking, transition and drinking regions (1, 2 and 3, respectively) of butterfly proboscises (figure 5). Means in columns within species followed by the same letter are not significantly different ($p > 0.05$; Tukey-HSD)

Species	*n*	feeding guild	region	dorsal legulae width (upper branch only)	single galea width
Danaus plexippus	7	nectar	1	21.5 ± 1.0c	124.1 ± 1.4a
			2	31.7 ± 1.5b	117.3 ± 1.6b
			3	42.4 ± 1.3a	107.6 ± 0.7c
Papilio glaucus	4	nectar	1	39.7 ± 1.5c	167.3 ± 3.5a
			2	50.5 ± 1.6b	156.2 ± 3.1b
			3	57.9 ± 1.7a	133.6 ± 3.0c
Vanessa cardui	4	nectar	1	12.3 ± 0.6c	109.3 ± 3.3a
			2	19.2 ± 1.6b	101.9 ± 2.6a
			3	33.0 ± 1.7a	92.6 ± 1.5b
Polygonia interrogationis	6	sap	1	13.9 ± 0.4c	148.7 ± 2.8a
			2	34.1 ± 2.3b	125.5 ± 1.5b
			3	56.9 ± 0.6a	105.2 ± 1.1c
Limenitis arthemis astyanax	4	sap	1	18.2 ± 2.6c	261.1 ± 2.6a
			2	68.0 ± 4.8b	237.3 ± 3.0b
			3	92.4 ± 1.3a	188.7 ± 3.3c

where $Z(\mu_0) = Z_0$ is the dimensionless meniscus height and K is an unknown constant.

Outer expansion. In this case, we seek a solution to equations (4.4)–(4.6) as $X^2 + Y^2 \to \infty$ where the ellipses of the elliptical system of coordinates transform to the circles. This solution has been considered in detail by Lo [28]. Rewriting equation (4.6) in cylindrical coordinates, $r = (X^2 + Y^2)^{1/2}$, we obtain $(1/r)(\mathrm{d}^2/\mathrm{d}r)(r(\mathrm{d}z/\mathrm{d}r)) - \varepsilon Z = 0$. This equation has the solution

$$Z = CK_0((\varepsilon X^2 + \varepsilon Y^2)^{1/2}), \tag{6.5}$$

where $K_0(x)$ is the modified Bessel function and C is an unknown constant. Solution (6.5) satisfies the boundary condition at infinity, but it does not satisfy the boundary condition at the fibre

surface. As we move closer to the fibre surface, i.e. X,Y become of the order of 1, equation (6.5) can be approximated by the first two terms of its asymptotic expansion

$$Z \cong -C \ln \frac{(\varepsilon X^2 + \varepsilon Y^2)^{1/2} e^{\gamma}}{2}, \tag{6.6}$$

where $\gamma = 0.577215$ is the Euler constant.

To confirm that the inner solution has a correct logarithmic behaviour at infinity, we note that the Cartesian (X,Y) coordinates at infinity are expressed through the elliptical coordinates (μ, v) as $\mu \to \infty$ in the following asymptotic form:

$$X \approx \left(\frac{H}{2}\right) \exp \mu \cos v \quad \text{and} \quad Y \approx \left(\frac{H}{2}\right) \exp \mu \sin v. \tag{6.7}$$

Solving these equations for μ, we find

$$X^2 + Y^2 \approx \left(\frac{H}{2}\right)^2 \exp(2\mu) \quad \text{or} \quad \mu = \left(\frac{1}{2}\right) \ln\left(\frac{4X^2 + 4Y^2}{H^2}\right) \quad \text{as } X^2 + Y^2 \to \infty. \tag{6.8}$$

Substituting this formula in equation (6.4), we obtain

$$Z = K\left\{\left(\frac{1}{2}\right) \ln\left(\frac{4X^2 + 4Y^2}{H^2}\right) - \mu_0\right\} + Z_0 \quad \text{as } X^2 + Y^2 \to \infty. \tag{6.9}$$

We need to match this solution with the inner solution by matching the factors K and C.

Matching condition. Thus, the outer and inner solutions have correct logarithmic behaviour, i.e. the inner solution can be matched with the outer solution if we set

$$K = -C, \quad \left(\frac{K}{2}\right) \ln\left(\frac{4}{H^2}\right) - \mu_0 K + Z_0 = \left(\frac{K}{2}\right) \ln\left(\frac{\varepsilon e^{2\gamma}}{4}\right). \tag{6.10}$$

Equation (6.10) allows one to express the constant K through the meniscus height Z_0,

$$K = \frac{Z_0}{(1/2) \ln(\varepsilon H^2 e^{2\gamma}/16) + \mu_0.} \tag{6.11}$$

Meniscus height Z_0 can be expressed through the average contact angle θ using equation (4.5). The integral over the meniscus profile can be evaluated as

$$\int \varepsilon Z \, \mathrm{d}x \, \mathrm{d}y = \varepsilon \int Z^{\text{inner}} \, \mathrm{d}x \, \mathrm{d}y + \varepsilon \int Z^{\text{outer}} \, \mathrm{d}x \, \mathrm{d}y. \tag{6.12}$$

The first integral is taken over the inner region closer to the proboscis surface and written in elliptic coordinates as

$$\int Z^{\text{inner}} \mathrm{d}x \, \mathrm{d}y = H \int_{\mu_0}^{M} \int_0^{2\pi} (\sinh^2 \mu + \sin^2 v)^{1/2} \times \int \{K(\mu - \mu_0) + Z_0\} \mathrm{d}\mu \, \mathrm{d}v. \tag{6.13}$$

According to the techniques of matched asymptotic expansions [51], it is not necessary to specify the exact value of the upper limit M. This value is taken in the region where the inner and outer solutions match, i.e. within the region where the ellipses of the elliptical system of coordinates transform into circles of the cylindrical coordinates. For us it is important to note that the upper limit M is of the order of 1, $\mathrm{M} \sim \mathrm{O}(1)$; therefore, the entire integral $\varepsilon \int Z^{\text{inner}} \mathrm{d}A$ is expected to be small, $\varepsilon \int Z^{\text{inner}} \mathrm{d}A \propto \varepsilon \ln \varepsilon \ll 1$. The second integral corresponding to the outer region of the asymptotic expansion can be evaluated in the cylindrical system of coordinates. As the lower integration limit R we choose the circle asymptotically corresponding to the ellipse $\mu = \mathrm{M}$:

$$\varepsilon \int Z^{\text{outer}} \mathrm{d}x \, \mathrm{d}y = -2\pi\varepsilon K \int_R^{\infty} K_0(r\sqrt{\varepsilon}) r \mathrm{d}r = -2\pi K \int_{\sqrt{\varepsilon} R}^{\infty} u K_0(u) \, \mathrm{d}u = 2\pi\sqrt{\varepsilon} K R K_1(R\sqrt{\varepsilon})$$

Taking into account the asymptotic approximation of the modified Bessel function of the second kind, $K_1(R\sqrt{\varepsilon}) \approx \Gamma(1)/R\sqrt{\varepsilon} = 1/R\sqrt{\varepsilon}$, we obtain

$$\varepsilon \int Z^{\text{outer}} \mathrm{d}x \, \mathrm{d}y \approx 2\pi K. \tag{6.14}$$

Thus, we have

$$-l \cos\theta = 2\pi K = \frac{2\pi Z_0}{(1/2) \ln(\varepsilon H^2 e^{2\gamma}/16) + \mu_0}. \tag{6.15}$$

Solving for Z_0, we obtain

$$Z_0 = -\left(\frac{l}{2\pi}\right) \cos\theta \left[\left(\frac{1}{2}\right) \ln\left(\frac{\varepsilon H^2 e^{2\gamma}}{16}\right) + \mu_0\right]. \tag{6.16}$$

The dimensionless perimeter of an ellipse is $l = 4E(\sqrt{1 - (b/a)^2})$, where E is the complete elliptic integral of the second kind. In a limiting case of a circular cylinder, $a = b$, when $l = 2\pi$, equation (6.16) reproduces the Lo solution $Z_0 = -\cos\theta \ln(\sqrt{\varepsilon} e^{\gamma}/2)$ [28]. Equation (6.16) can be further simplified taking into account the smallness of the complementary angle $\delta = \theta - \pi/2$, $|\delta| \ll 1$ at the boundary of the drinking region. Using equation $\cos\theta = \cos((\pi/2) - (\pi/2) + \theta) = \cos((\pi/2) + \delta) \approx -\delta$, equation (6.16) is rewritten as $Z_0 = (l\delta/2\pi)[(1/2) \ln(\varepsilon H^2 e^{2\gamma}/16) + \mu_0]$, which corresponds to the following dimensional height

$$z_0 = \left(\frac{a\delta l}{2\pi}\right) \ln\left[\frac{(1 + b/a)\sqrt{\varepsilon} e^{\gamma}}{4}\right], \tag{6.17}$$

where a is a proboscis semi-axis at the transition region given in table 1.

The meniscus profile near the fibre is described by equation (6.4), $Z = K(\mu - \mu_0) + Z_0$, which is represented in a dimensional form as $z = (al\delta/2\pi)(\mu - \mu_0) + z_0$.

We acknowledge support from National Science Foundation grant EFRI 0937985. We thank the technicians at the Electron Microscope Facility and Terri Bruce at the Jordan Hall Imaging Facility (Clemson University, SC) for assistance in SEM and fluorescent imaging, respectively.

References

1. Adler PH, Foottit RG. 2009 *Insect biodiversity: science and society*. Chichester: Wiley-Blackwell.
2. Grimaldi D, Engel MS. 2005 *Evolution of the insects*. New York, NY: Cambridge University Press.
3. Karolyi F, Gorb SN, Krenn HW. 2009 Pollen grains adhere to the moist mouthparts in the flower visiting beetle *Cetonia aurata* (Scarabaeidae, Coleoptera). *Arthropod-Plant Interact.* **3**, 1–8. (doi:10.1007/s11829-008-9052-5)
4. Vincent JFV, Wegst UG. 2004 Design and mechanical properties of insect cuticle. *Arthropod Struct. Dev.* **33**, 187–199. (doi:10.1016/j.asd.2004.05.006)
5. Rudall KM, Kenchington W. 1973 The chitin system. *Biol. Rev. Camb. Philos. Soc.* **48**, 597–633.
6. Merzendorfer H. 2006 Insect chitin synthases: a review. *J. Comp. Physiol. B Biochem. Syst. Environ. Physiol.* **176**, 1–15. (10.1007/s00360-005-0005-3)
7. Adamson AW, Gast AP. 1997 *Physical chemistry of surfaces*, 6th edn. New York, NY: Wiley.
8. Forbes P. 2008 Self-cleaning materials: lotus leaf-inspired nanotechnology. *Sci. Am.*

299, 88–95. (doi:10.1038/scientificamerican 0808-88)

9. Byun D, Hong J, Saputra, Ko JH, Lee YJ, Park HC, Byun B-K, Lukes JR. 2009 Wetting characteristics of insect wing surfaces. *J. Bionic Eng.* **6**, 63–70. (doi:10.1016/S1672-6529(08)60092-X)
10. Eastham LES, Eassa YEE. 1955 The feeding mechanism of the butterfly *Pieris brassicae* L. *Phil. Trans. R. Soc. Lond. B* **239**, 1–43. (doi: 10.1098/ rstb.1955.0005)
11. Kingsolver JG, Daniel TL. 1995 Mechanics of food handling by fluid-feeding insects. In *Regulatory mechanisms in insect feeding* (eds RF Chapman, G de Boer), pp. 32–74. New York, NY: Springer.
12. Monaenkova D, Lehnert MS, Andrukh T, Beard CE, Rubin B, Tokarev A, Lee W-K, Adler PH, Kornev KG. 2012 Butterfly proboscis: combining a drinking straw with a nanosponge facilitated diversification of feeding habits. *J. R. Soc. Interface* **9**, 720–726. (doi: 10.1098/rsif.2011.0392)
13. Holdgate MW. 1955 The wetting of insect cuticles by water. *J. Exp. Biol.* **32**, 591–617. (doi:10.1017/ S0007485300027528)
14. Vogel S. 2003 Comparative biomechanics: life's physical world. Princeton, NJ: Princeton University Press.
15. Genzer J, Marmur A. 2008 Biological and synthetic self-cleaning surfaces. *MRS Bulletin* **33**, 742–746.
16. Krenn HW. 2010 Feeding mechanisms of adult Lepidoptera: structure, function, and evolution of the mouthparts. *Annu. Rev. Entomol.* **55**, 307–327. (doi:10.1146/annurev-ento-112408-085338)
17. Knopp MCN, Krenn HW. 2003 Efficiency of fruit juice feeding in *Morpho peleides* (Nymphalidae, Lepidoptera). *J. Insect Behav.* **16**, 67–77. (doi:10. 1023/A:1022849312195)
18. Mollemann F, Krenn HW, Van Alphen ME, Brakefield PM, Devries PJ, Zwann BJ. 2005 Food intake of fruit-feeding butterflies: evidence for adaptive variation in proboscis morphology. *Biol. J. Linn. Soc.* **86**, 333–343. (doi:10.1111/j.1095-8312.2005.00533.x)
19. Krenn HW, Zulka KP, Gatschnegg T. 2001 Proboscis morphology and food preferences in nymphalid butterflies (Lepidoptera: Nymphalidae). *J. Zool. Lond.* **254**, 17–26. (doi:10.1017/ S0952836901000528)
20. Edney EB. 1977 *Water balance in land arthropods*. New York, NY: Springer.
21. Hadley NF. 1994 *Water relations of terrestrial arthropods*. New York, NY: Academic Press.
22. Parker AR, Lawrence CR. 2001 Water capture by a desert beetle. *Nature* **414**, 33–34. (doi:10.1038/ 35102108)
23. Gao XF, Jiang L. 2004 Water-repellent legs of water striders. *Nature* **432**, 36–36. (doi:10.1038/432036a)
24. Bush JWM, Hu DL, Prakash M. 2007 The integument of water-walking arthropods: form and function. *Adv. Insect Physiol.* **34**, 117–192.
25. Zheng YM, Bai H, Huang Z, Tian X, Nie F-Q, Zhao Y, Zhai J, Jiang L. 2010 Directional water collection on wetted spider silk. *Nature* **463**, 640–643. (doi:10. 1038/nature08729)
26. White DA, Tallmadge JA. 1965 Static menisci on the outside of cylinders. *J. Fluid Mech.* **23**, 325–335. (doi:10.1017/S0022112065001398)
27. Carroll BJ. 1976 The accurate measurement of contact angle, phase contact areas, drop volume, and Laplace excess pressure in drop-fiber systems. *J. Coll. Interf. Sci.* **57**, 488–495. (doi:10.1016/0021-9797(76)90227-7)
28. Lo LL. 1973 The meniscus on a needle—a lessson in matching. *J. Fluid Mech.* **132**, 65–78. (doi:10. 1017/S0022112083001470)
29. Tsai CC *et al*. 2011 Nanoporous artificial proboscis for probing minute amount of liquids. *Nanoscale* **3**, 4685–4695. (doi:10.1039/c1nr10773a)
30. Cassie ABD, Baxter S. 1944 Wettability of porous surfaces. *Trans. Faraday Soc.* **40**, 546–551.
31. Quéré D. 2008 Wetting and roughness. *Annu. Rev. Mater. Res.* **38**, 71–99.
32. Liu K, Yao X, Jiang L. 2010 Recent developments in bio-inspired special wettability. *Chem. Soc. Rev.* **39**, 3240–3255.
33. Bhushan B, Jung YC. 2011 Natural and biomimetic artificial surfaces for superhydrophobicity, self-cleaning, low adhesion, and drag reduction. *Prog. Mater. Sci.* **56**, 1–108.
34. Gao LC, McCarthy TJ, Zhang X. 2009 Wetting and superhydrophobicity. *Langmuir* **25**, 14 100–14 104.
35. Cassie ABD. 1948 Contact angles. *Discuss. Faraday Soc.* **3**, 11–16. (doi:10.1039/DF9480300011)
36. Marmur A. 2011 Measures of wettability of solid surfaces. *Eur. Phys. J. Special Topics* **197**, 193–198. (doi:10.1140/epjst/e2011-01457-4)
37. Marmur A, Bittoun E. 2009 When Wenzel and Cassie are right: reconciling local and global considerations. *Langmuir* **25**, 1277–1281. (doi:10. 1021/la802667b)
38. Adam NK. 1937 Detergent action and its relation to wetting and emulsification. *J. Soc. Dyers Colour.* **53**, 121–129. (doi:10.1111/j.1478-4408.1937. tb01955.x)
39. McHale G, Newton MI. 2002 Global geometry and the equilibrium shapes of liquid drops on fibers. *Colloids Surf. A: Physicochem. Eng. Asp.* **206**, 79–86. (doi:10.1016/S0927-7757(02)00081-X)
40. Bico J, Thiele U, Quéré D. 2002 Wetting of textured surfaces. *Colloid Surf. A Physicochem. Eng. Asp.* **206**, 41–46. (doi.org/10.1016/S0927-7757(02)00061-4)
41. Sun MX, Watson GS, Zheng YM, Watson JA, Liang AP. 2009 Wetting properties on nanostructured surfaces of cicada wings. *J. Exp. Biol.* **212**, 3148–3155. (doi:10.1242/jeb.033373)
42. Watson GS, Cribb BW, Watson JA. 2010 The role of micro/nano channel structuring in repelling water on cuticle arrays of the lacewing. *J. Struct. Biol.* **171**, 44–51. (doi:10.1016/j.jsb.2010.03.008)
43. Hu HMS, Watson GS, Cribb BW, Watson JA. 2011 Non-wetting wings and legs of the cranefly aided by fine structures of the cuticle. *J. Exp. Biol.* **214**, 915–920. (doi:10.1242/jeb.051128)
44. Krenn HW, Kristensen NP. 2000 Early evolution of the proboscis of Lepidoptera: external morphology of the galea in basal glossatan moths lineages, with remarks on the origin of the pilifers. *Zool. Anz.* **239**, 179–196.
45. Krenn HW, Plant J, Szucsich NU. 2005 Mouthparts of flower-visiting insects. *Arthropod Struct. Dev.* **34**, 1–40. (doi:10.1016/j.asd.2004.10.002)
46. Grant J, Djani D, Lehnert MS. 2012 Functionality of a reduced proboscis: fluid uptake by *Phigalia strigataria* (Minot) (Geometridae: Ennominae). *J. Lepid. Soc.* **66**, 211–215.
47. Krenn HW. 1990 Functional morphology and movements of the proboscis of Lepidoptera (Insecta). *Zoomorphology* **110**, 105–114. (doi:10. 1007/BF01632816)
48. Bauder JAS, Lieskonig NR, Krenn HW. 2011 The extremely long-tongued Neotropical butterfly *Eurybia lycisca* (Riodinidae): proboscis morphology and flower handling. *Arthropod Struct. Dev.* **40**, 122–127. (doi:10.1016/j.asd.2010.11.002)
49. Karolyi F, Szucsich NU, Colville JF, Krenn HW. 2012 Adaptations for nectar-feeding in the mouthparts of long-proboscid flies (Nemestrinidae: *Prosoeca*). *Biol. J. Linn. Soc.* **107**, 414–424. (doi:10.1111/j. 1095-8312.2012.01945.x)
50. Fowler SD, Greenspan P. 1985 Application of Nile Red, a fluorescent hydrophobic probe, for the detection of neutral lipid deposits in tissue sections: comparison with Oil Red O. *J. Histochem. Cytochem.* **33**, 833–836. (doi:10.1177/33.8.4020099)
51. Bender CM, Orszag SA. 1999 *Advanced mathematical methods for scientists and engineers: asymptotic methods and perturbation theory*. New York, NY: Springer.